Available online at www.sciencedirect.com

SciVerse ScienceDirect

Ceramics International 39 (2013) 5695–5704

CERAMICS INTERNATIONAL

www.elsevier.com/locate/ceramint

# Dielectric and impedance spectroscopy of zirconium modified $(Na_{0.5}Bi_{0.5})TiO_3$ ceramics

B.K. Barick[a,1], R.N.P. Choudhary[b], D.K. Pradhan[a,*]

[a]Department of Physics, National Institute of Technology, Rourkela 769008, India
[b]Department of Physics, ITER, Siksha 'O' Anusandhan University, Bhubaneswar 751030, India

Received 2 November 2012; received in revised form 25 December 2012; accepted 29 December 2012
Available online 16 January 2013

**Abstract**

Preliminary structural and detailed dielectric and electrical properties of zirconium (Zr) modified-sodium bismuth titanate (i.e., $Na_{0.5}Bi_{0.5}Ti_{1-x}Zr_xO_3$(NBZT)) ceramics were studied. Structural analysis of the materials with room temperature X-ray diffraction data confirmed the formation of compounds in the rhombohedral crystal system. SEM micrographs of the compounds showed the abnormal grain growth but with better densification and homogeneity on substitution of Zr at the Ti site. Dielectric and complex impedance spectroscopic studies were carried out in a wide frequency (i.e., $10^2$–$10^6$ Hz) and temperature (30–500 °C) range. The maximum permittivity (at transition temperature) was found to be decreased on increasing Zr concentration in NBZT but the diffuseness of dielectric peak increases. The nature of frequency dependence of ac conductivity of NBZT follows the Jonscher power law, and calculated dc conductivity follows Arrhenius behavior. Detailed studies of complex impedance spectroscopy have provided better understanding of: (i) relaxation process and (ii) microstructure-properties relationship in the materials. Complex impedance and modulus spectra confirm the significant contribution of both grain and grain boundary to electrical response of the materials. It is observed that relaxation processes in the materials are of non-Debye type.


*Keywords:* A. Powders: solid state reaction; C. Dielectric properties; C. Electrical properties; D. $BaTiO_3$; Titanates

## 1. Introduction

Since the discovery of ferroelectric phenomena in perovskite $BaTiO_3$ (BT) in 1940s [1], a large number of oxides of different structural families were examined to get the behavior of the materials. Among all the ferroelectric oxides studied so far, some perovskite oxides were found to be useful for some solid state electronic devices such as random access memory devices, high dielectric constant capacitor, pyro-electric detectors, imaging devices, electro-optic devices, modulators etc. [1,2]. Among the studied ferroelectric oxides, some lead based ferroelectric oxides such as lead titanate, lead zirconium titanate etc. are found to be most suitable for fabrication of various solid state devices. Unfortunately, because of the toxic nature they produce environmental pollutions [3]. Therefore, attempts are now being made to search lead free new ferroelectric materials which can be a replacement of lead based ferroelectrics without losing much of their physical properties required for devices. $Na_{0.5}Bi_{0.5}TiO_3$ (NBT) is one of such lead free ferroelectric materials. It belongs to the A-site disordered-pervoskite ferroelectric family which has attracted a significant research interests in recent years. It is ferroelectric at room temperature with a large remnant polarization (38 μC/cm$^2$) and high Curie temperature (320 °C) [4]. Also, as Bi has iso-electronic configuration to Pb, it causes high polarization (as in lead based ferroelectric materials) due to the presence of stereo-chemically active lone pair electrons. This situation projects NBT as a promising lead-free ferroelectric material. However, there are some problems of NBT such as high dielectric loss, high conductivity, low depolarization temperature ($T_d$) and high coercive field (73 kV/cm) which limits the material to

*Corresponding author. Tel.: +91 661 2462729.
*E-mail address:* dillip.pradhan79@gmail.com (D.K. Pradhan).
[1]Present address: Department of Physics, Indian Institute of Technology, Bombay 400076, India.

0272-8842/$ - see front matter © 2013 Elsevier Ltd and Techna Group S.r.l. All rights reserved.
http://dx.doi.org/10.1016/j.ceramint.2012.12.087

be used for devices. There are various ways to solve these problems and enhance electrical properties. One of the possible ways to solve the above problems is by making solid-solutions of two similar types of perovskites (near morphotropic phase boundaries) or modifying the base compound with suitable substitutions. Mostly solid solutions of NBT-BT, NBT-BKT ($K_{0.5}Bi_{0.5}TiO_3$), etc., have been studied. Though increment of piezoelectric properties was observed near MPB composition of NBT-BT but the reduction of depolarization temperature ($T_d$) occurs at MPB, which again limits its application because of the decrease of ferroelectric properties above $T_d$ [5]. Also, numerous amount of works are still going on to modify NBT by suitable substitutions at the A and/or B sites. Zhang et al. [6] studied the substitution of zinc in NBT results in decreased $T_d$ and enhanced relaxor behavior. La modified NBT showed three phase transitions ($T_d$, $T_{R-O}$, $T_m$) with reduction of $T_d$, increment of $T_m$ and broadening of dielectric peak studied by Barick et al. [7]. The piezoelectric constant of Zr modified NBT was studied by Watcharapasorn and Jiansirisomboon [8] and it reduced with increasing of Zr concentration. Yuan et al. [9] reported the reduction of ferroelectric properties in Ca modified NBT, but improvement of dielectric properties has been observed on further doping of Mn in Ca modified NBT. Yamada et al. [10] studied the structural phase relationship in the $[(K_{1/2}Bi_{1/2})_{1-y}(Na_{1/2}Bi_{1/2})_y](Ti_{1-x}B_x)O_3$ system with B=Zr, $Fe_{1/2}Nb_{1/2}$, $Zn_{1/3}Nb_{2/3}$ or $Mg_{1/3}Nb_{2/3}$ using XRD and dielectric measurements. They have reported that the phase is unidentified above 60% Zr in NBT. Lily et al. [11,12] studied electrical properties of 25% Zr modified NBT and $(Na_{0.5}Bi_{0.5})ZrO_3$ (NBZ) using impedance spectroscopy method. NBZ showed orthorhombic crystal structure with transition temperature ($T_c$) at 425 °C. $ZrO_2$ substituted NBT has been studied by Kumari et al. [13]. They showed the increment of $T_c$ and $T_d$ (depolarization temperature) to high temperature as compared to that of NBT. $(Bi_{1/2}Na_{1/2})_{1-x}Ba_xZr_yTi_{1-y}O_3$ single crystal showed the high values of electro-strictive strain as reported by Sheets et al. [14]. Rachakom et al. [15] observed the phase transition from rhombohedral to an orthorhombic structure on addition of Zr in NBT by X-ray diffraction analysis. Aksel et al. [16] reported that Fe-modified NBT (at low Fe concentration) increases $T_d$ but decreases with higher Fe content without change of the structure of the material. Substitution of Mn and Fe behaved as soft dopant whereas La substitution behaved as hard dopant similar to that of PZT [17]. The solid solution of NBT-BA ($BiAlO_3$) ceramics studied by Yu and Ye [18] and they showed some improvement in ferroelectric and piezoelectric properties of the compound as compared to those of NBT.

It has also been reported that substitution of isovalent element(s) reduces the dielectric loss, lowers the compliance and inhibits domain reorientations of the material [19]. Moreover, modification of the B-site of pervoskite ferroelectrics material plays the crucial role in monitoring the electrical properties of the materials. Among the various modifier, zirconium is known for the development of high quality materials on substituting at the B-site e.g. $Pb(Zr_{1-x}Ti_x)O_3$ and $Ba(Zr_{1-x}Ti_x)O_3$ ceramics. Hence, substitution of Zr at the Ti-site was considered to be a suitable approach to modify the properties of pervoskite NBT ferroelectric ceramics. As $Zr^{4+}$ is isovalent to $Ti^{4+}$, it does not have alterable valence and would not generate any additional charge carriers. On the other hand, $Zr^{4+}$ ion is chemically more stable than $Ti^{4+}$ and the ionic radius of $Zr^{4+}$ (0.087 nm) is larger than that of $Ti^{4+}$ (0.068 nm), so the B-site $Zr^{4+}$ substitutions could enhance the relative ionic displacement by expansion of the perovskite lattice. The substitution of Ti by Zr would depress the conduction by electronic hopping between $Ti^{4+}$ and $Ti^{3+}$ oxidation states. It is reported that an increase in the Zr content decreases the relative dielectric permittivity ($\varepsilon_r$), maintaining a low and stable leakage current in ferroelectric materials [20]. Detailed literature survey shows that there are only few reports available on the Zr-modified NBT, and those are limited to only structural and piezoelectric properties [8,10]. The effect of Zr substitution on dielectric and electric conduction behavior of $(Na_{0.5}Bi_{0.5})TiO_3$ ceramics requires further studies (with various percentages of Zr substitutions in NBT). In the present study, Zr modified NBT have been prepared by a high-temperature solid-state reaction route. Preliminary structural/micro-structural, dielectric and resistive properties of the Zr modified NBT ceramics have been studied using dielectric and impedance spectroscopic method to get better understanding of (i) the electrical conduction and dielectric relaxation mechanism and (ii) microstructure-electrical properties relationship of the materials as a function of temperature and frequency.

## 2. Experimental procedures

The polycrystalline samples of $(Na_{0.5}Bi_{0.5})Ti_{(1-x)}Zr_xO_3$, ($x=0.00$, 0.05, 0.1, 0.2, and 0.3) were prepared by a high-temperature solid-state reaction technique using high-purity (>99.9%) oxides ($Bi_2O_3$, $TiO_2$, and $ZrO_2$) and carbonate ($Na_2CO_3$) (all from M/s LOBA Chemie Private Limited). The stoichiometric amounts of the precursor powders were mixed using agate mortar and pestle first in air and then in wet (acetone) medium to get a homogeneous mixture of the compounds. The calcination of the above mixtures was carried out at an optimized temperature (950 °C) and time (4 h). Then the calcined powders were grinded and further calcined at 1000 °C for 4 h to ensure the completion of reaction and formation of desired compounds. The fine calcined powders were mixed with binder (Polyvinyl alcohol (PVA)) and compacted by a hydraulic press to form pellets of 10 mm diameter and 1–2 mm thickness at a pressure of $6\times10^7$ kg/cm$^2$. The sintering of the pellet samples was carried out at 1080 °C for 4 h.

In order to confirm the formation of Zr-modified NBT through preliminary structural analysis, X-ray diffraction

(XRD) data were collected at room temperature by X-ray diffractometer (PANalytical's X'Pert PRO diffractometer) with Cu-$K_{\alpha 1}$($\lambda = 1.54{,}181$ Å) radiation from 20° to 80° with a scan rate of 2°/min. The surface morphology and grain size of the samples were studied using scanning electron microscope (SEM) (JSM-6480 LV, JEOL) at room temperature on platinum coated pellets. The sintered pellets were first polished and then coated with silver paste on both surfaces as electrode for electrical measurement. The silver electrode samples were dried at 150 °C for 12 h to remove the moisture, if any. The dielectric and impedance parameters were obtained using a LCR meter (model 3532-50, LCR HiTESTER, Hioki, Japan) in wide frequency range ($10^2$–$10^6$ Hz) at different temperatures (30–500 °C).

## 3. Results and discussion

### 3.1. Structural and microstructural studies

Fig. 1 I(a–e) compares the XRD patterns of calcined powder of $(Bi_{0.5}Na_{0.5})Ti_{1-x}Zr_xO_3$, $x=0$, 0.05, 0.1, 0.2, 0.3 at room temperature. The sharp diffraction peaks in the XRD pattern of the compounds, which are different from those of ingredients, suggest the formation of the compounds with a small amount of secondary phase (shown by asterisk mark). The impurity peak corresponds to the reflection of $ZrO_2$ (ICDD no. 80-0966). The amount of secondary phase increases with rise in Zr content. The peak position ($2\theta$), full width at half maximum (FWHM), and intensity were calculated using commercially available software (PEAK FIT) for each peak of the XRD pattern. Indexing of all the peaks of XRD patterns were carried out using diffraction angle ($2\theta$) and intensity of each peak by least-squares method with the help of standard computer program (POWD) [21]. The best agreement between the observed (obs) and calculated (cal) interplanar spacing ($d$) and Bragg angles was found in rhombohedral crystal structure ($R3c$ space group) with hexagonal axis. As Zr concentration increases the XRD peak shifted to lower $2\theta$ values (higher $d$ spacing). This may be due to the substitution of higher ionic radius element (Zr) at the lower ionic radius element (Ti). The small intensity peak around 38° corresponds to the super-lattice reflection of NBT compound [22]. The super-lattice reflection of $(Bi_{0.5}Na_{0.5})Ti_{1-x}Zr_xO_3$, $x=0$, 0.05, 0.1, 0.2, 0.3 at room temperature has been shown in Fig. 1II (a–e). The super-lattice reflection peak is well observed in case of NBT and 5% Zr modified NBT. The intensity found to be decreased for 10%, 20%, and 30% Zr modified NBT. The super-lattice reflection indicates the anti-phase rotation $a^-a^-a^-$ (characteristic tilting feature of $R3c$ space group) which confirms the $R3c$ space group rather $R3m$ [17]. Weak intensity of super-lattice reflection suggests that the distortion from ideal cubic cell is small, and it decreases on increasing Zr content. The Williamson–Hall method [23] was used to calculate the crystallite size and rms strain of the NBT and modified NBT samples using the following equation: $(\beta\cos\theta/\lambda)^2 = (1/D)^2 + (4\varepsilon\sin\theta/\lambda)^2$ where $\beta$ is the FWHM of XRD peaks, and it was calculated after subtracting the FWHM of standard polycrystalline silicon peak from the observed FWHM of sample peak, $D$ and $\varepsilon$ are particle size and rms strain, respectively. The lattice parameters, unit cell volume, crystallite size, and root mean square (rms) strain of the materials are presented in Table 1. The particle size of Zr modified NBT increases with increase in Zr content (Table 1).

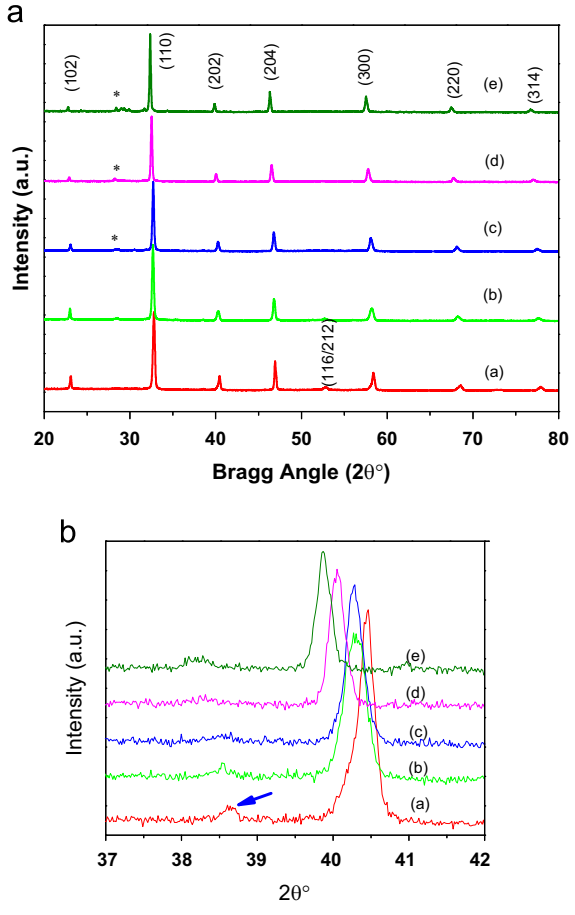


Fig. 1. (I, II) XRD pattern and superlattice reflection of $(Na_{0.5}Bi_{0.5})Ti_{(1-x)}Zr_xO_3$, (a) $x=0.0$, (b) $x=0.05$, (c) $x=0.1$, (d) $x=0.2$, (e) $x=0.3$.

The SEM micrographs of NBT and 10%, 20%, and 30% Zr modified NBT sintered pellets are shown in Fig. 2. The nature of SEM micrographs shows the polycrystalline characteristics of samples. The sample surfaces consist of non-uniform distribution of nearly rectangular grain of

Table 1
Comparison of lattice parameters ($a$ and $c$), unitcell volume ($V$), particle size ($D$), and rms strain ($\varepsilon_{rms}$) of Zr modified NBT.

| Sample | $a$ (Å) | $c$ (Å) | $V$ (Å$^3$) | $D$ (nm) | $\varepsilon_{rms}$ ($<\varepsilon^2>^{1/2}$) |
|---|---|---|---|---|---|
| 5 % Zr NBT | 5.5037(16) | 13.4870(16) | 353.799 | 165 | 0.00385 |
| 10 % Zr NBT | 5.5210(50) | 13.5219(50) | 356.951 | 136 | 0.00251 |
| 20 % Zr NBT | 5.5465(56) | 13.5901(56) | 362.067 | 172 | 0.00230 |
| 30 % Zr NBT | 5.5607(34) | 13.6211(34) | 364.761 | 183 | 0.00195 |

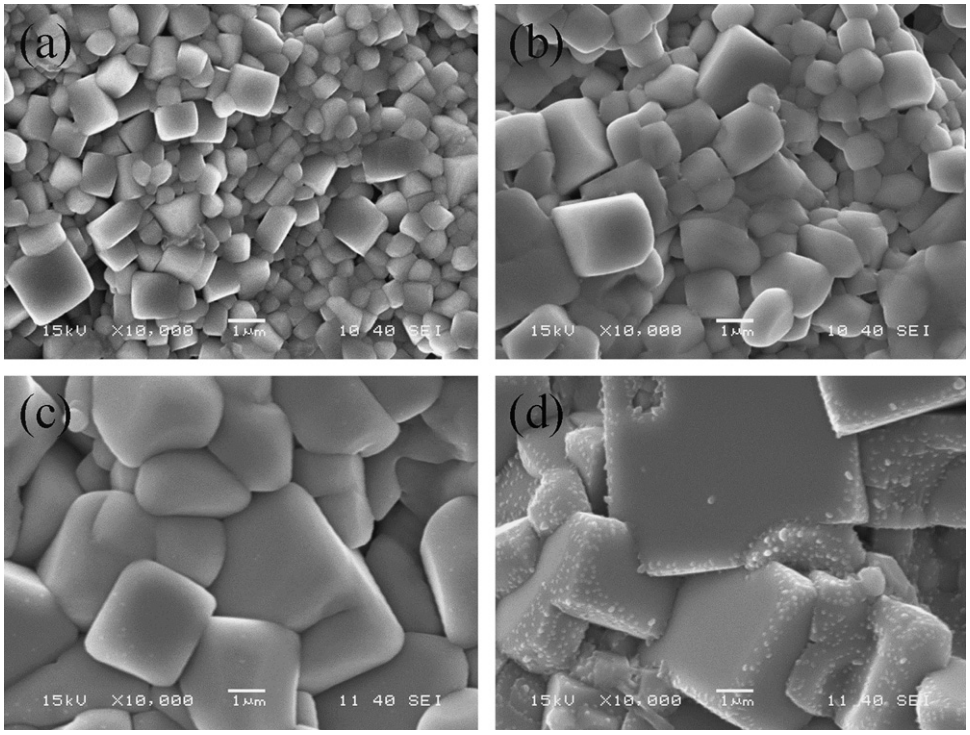


Fig. 2. SEM micrographs of $(Na_{0.5}Bi_{0.5})Ti_{(1-x)}Zr_xO_3$, (a) $x=0.0$, (b) $x=0.1$, (c) $x=0.2$, (d) $x=0.3$.

different sizes. The grain size significantly increases from 0.5 to 3 μm on increasing Zr concentration from 0–30% in NBZT. The microstructure is generally densely packed, but few scattered pores are observed, which indicates that there is certain degree of porosity in the samples. The contrast small dots on the edges of grains (Fig. 2(e)) shows the presence of secondary phase on the surface which agrees well with the secondary peak observed in XRD (Fig. 1I (e)).

### 3.2. Dielectric studies

Fig. 3 shows the variation of dielectric constant with temperature at 1 MHz of NBT and 5%, 10%, 20%, 30% Zr modified NBT. It has been observed that dielectric constant increases with increase in temperature up to a maximum value ($\varepsilon_{max}$) and then it decreases. At low frequency (not shown) dielectric constant suddenly increases with rise in temperature just after the transition temperature (without showing any dielectric peak) which may be due to the increase of conductivity in samples due to presence of space charge polarization. The observed diffused dielectric anomaly (around 330 °C) represents the anti-ferroelectric to paraelectric phase transition. This peak is frequency independent. In addition, the maximum value of dielectric constant ($\varepsilon_{max}$) is reduced in all compositions (shown in dielectric constant versus temperature plot). The reduction in the value of dielectric constant may be due to the reduction of distortion in the unit cell which is evident from Fig. 1.II.

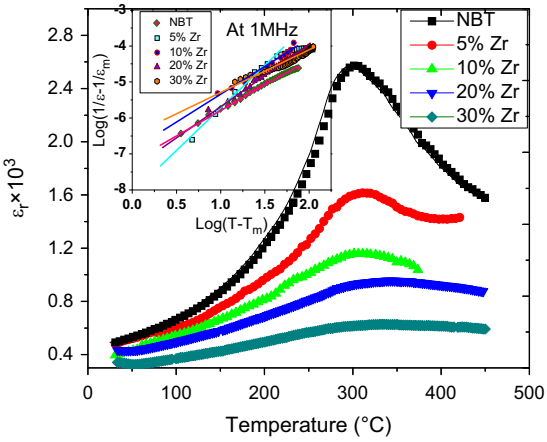


Fig. 3. Variation of dielectric constant with temperature at 1 MHz of $(Na_{0.5}Bi_{0.5})Ti_{(1-x)}Zr_xO_3$, $x=0.0$, 0.05, 0.1, 0.2, 0.3. Inset: diffusivity curves at 1 MHz.

An increase of Zr in NBZT shifts the transition temperature ($T_c$) of NBT towards the higher temperature side. This may be due to the increase in translational symmetry and the size of the polar region which modify the distribution of neighboring ions because of the comparatively large ionic radius of Zr cation [24]. The order of diffusivity or disorder in the samples can be analyzed by modified Curie–Weiss law as: $1/\varepsilon-1/\varepsilon_m=(T-T_m)^{\gamma}/C$,where $\gamma$ is the diffusivity, $C$ is the Curie–Weiss constant, $\varepsilon$ is dielectric constant at a given temperature $T$ and $\varepsilon_m$is its maximum value at $T_m$. Inset of Fig. 3 shows the diffusivity curve of NBT and Zr modified NBT at 1 MHz. The slope of the straight line gives the value

Table 2
Comparison of $\varepsilon_{max}$, $T_c$, $\gamma$ (at 1 MHz frequency), $E_a$ of NBT and Zr modifed NBT.

| Sample | $\varepsilon_{max}$ | $T_c$ (°C) | $\gamma$ | $E_a$ (eV) |
|---|---|---|---|---|
| NBT | 2573 | 301 | 1.58 | 0.81 |
| 5% Zr NBT | 1618 | 313 | 1.81 | 1.37 |
| 10% Zr NBT | 1160 | 311 | 1.59 | 1.56 |
| 20% Zr NBT | 955 | 345 | 1.73 | 1.19 |
| 30% Zr NBT | 627 | 338 | 1.37 | 0.65 |

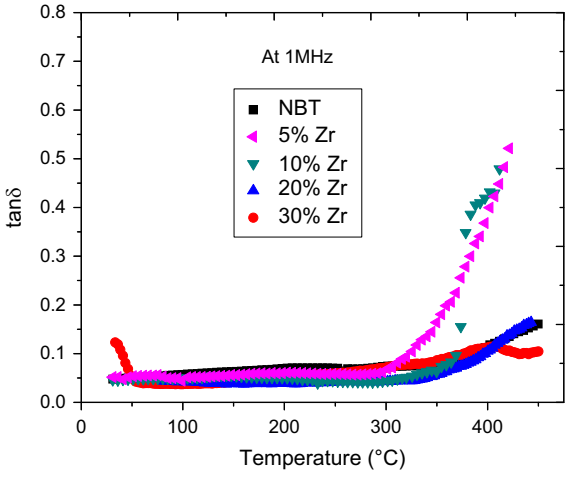


Fig. 4. Variation of tanδ with temperature at 1 MHz of $(Na_{0.5}Bi_{0.5})$-$Ti_{(1-x)}Zr_xO_3$, $x$=0.0, 0.05, 0.1, 0.2, 0.3.

of $\gamma$ and its value generally lies in between 1 and 2 ($1 \leq \gamma \leq 2$). The diffusion factor can be employed to describe the degree of diffusivity of the phase transitions. In case of $\gamma$ equals to unity, Curie–Weiss law is followed and it shows the normal ferroelectric phase transition. The value of $\gamma$ is equal to two for complete diffusive phase transitions. The transition temperature (calculated from $1/\varepsilon$ versus temperature plot) and value of $\gamma$ (calculated at 1 MHz) for NBZT samples are compared in Table 2. The value of $\gamma$ clearly showed that the phase transition is of diffuse type. The diffuse behavior of NBT may be due to A-site cations disorder in the material and defects. Disorder and defect induce the formation of micropolar regions, and each of such regions has its own transition temperatures.

Fig. 4 shows the variation of dielectric loss (tanδ) with temperature at 1 MHz for NBT and 5%, 10%, 20%, 30% Zr modified NBT. It is observed that the tangent loss increases with increase in temperature for all the frequencies. The increase in tanδ of Zr modified NBT is very small up to 300 °C, and above this temperature there is a sudden increase in its value with rise in temperature. The rapid increment in the value of tanδ at low frequency on the higher temperature side may be due to release of space charges [25]. The dielectric loss of the Zr modified NBT samples are nearly same as that of parent compounds at low temperatures.

### 3.3. Conductivity studies

Fig. 5(a–d) shows the variation of ac conductivity ($\sigma_{ac}$) with frequency at higher temperatures for 5%, 10%, 20%, and 30% Zr modified NBT ceramics. The $\sigma_{ac}$ was calculated from dielectric data using the following relation:$\sigma_{ac} = \varepsilon_0\varepsilon_r\omega\tan\delta$ where $\varepsilon_o$, $\varepsilon_r$, $\omega$, and tanδ are dielectric permittivity in vacuum, relative permittivity, angular frequency and dielectric loss, respectively. At low temperatures, the frequency dependence of ac conductivity shows the dispersion through the frequency range of investigation. At higher temperature, $\sigma_{ac}$ remains almost constant in the low frequency region as a result frequency independent plateau is seen, whereas the dispersion of conductivity is observed in the higher frequency region. The Jonscher power law is used to fit the ac conductivity of the material as follows: $\sigma_{ac}=\sigma_{dc}+A\omega^n$ where $\sigma_{dc}$ is frequency independent conductivity that related to dc conductivity, $A$ is the temperature dependent pre-exponential factor and $n$ is the frequency exponent. The value of $n$ varies between 0 and 1 [26]. In the conductivity versus frequency plots, the symbols denote the experimental data and solid line represents the power law fitted curves. There is very close agreement between the experimental data and the fitted solid line. The $A$, $n$, and $\sigma_{dc}$ are the fitted parameters. Two regions are observed in the conductivity spectrum. The long-range translational hoping conduction in low frequency region gives rise to dc conductivity ($\sigma_{dc}$). The frequency dependant short-range translational and localized hoping conduction at high frequency is assigning by $A\omega^n$ term. The cross over from the frequency independent region to the frequency dependent region shows the onset of the conductivity relaxation, which further indicates the transition from long range hopping to the short-range ionic motion. The onset of conductivity relaxation shifts to higher frequency side with rise in temperature. Jump relaxation model (JRM) may be used to explain the conduction mechanisms in solids [27]. At the low frequency region, the conductivity is mainly due to the substantial successful hopping of ions between different sites but hoping of ions reduces with increase of frequency. The change in the ratio of successful to unsuccessful hoping of ions results in dispersion of conductivity with increase in frequency. According to JRM, the different activation energies are associated with successful and unsuccessful hopping processes. The value of $\sigma_{ac}$ decreases with increase in the Zr concentration in NBT throughout the frequency range. At higher temperatures, the $\sigma_{ac}$ increases with temperature confirming the negative temperature coefficient of resistance (NTCR) behavior that is a typical characteristic of a semiconductor.

Fig. 6 shows the variation of dc conductivity with inverse of absolute temperature (i.e. $\ln\sigma_{dc}$ versus $10^3/T$). From the figure it is clear that the conductivity increases with increase in temperature. This temperature dependence of dc conductivity can be explained by the empirical relation: $\sigma=\sigma_p\exp(-E_a/kT)$, ($\sigma_p$=pre-exponential factor,

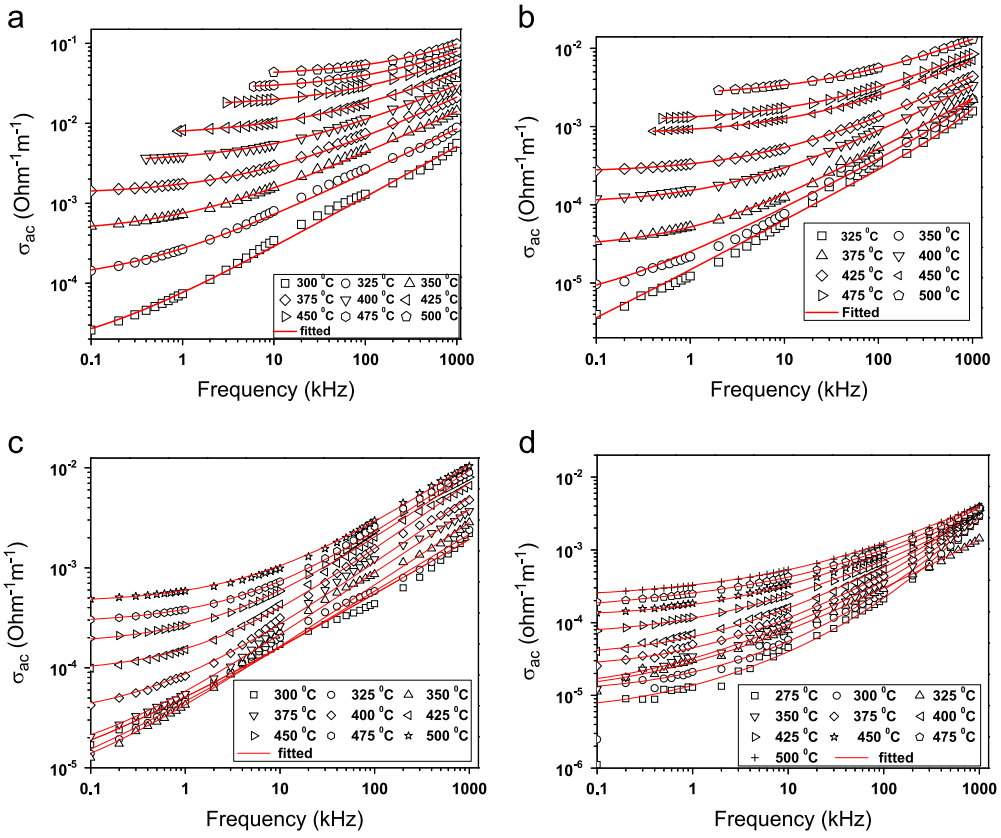


Fig. 5. Variation of ac conductivity with frequency at different temperatures of $(Na_{0.5}Bi_{0.5})Ti_{(1-x)}Zr_xO_3$, (a) $x=0.05$,(b) $x=0.1$, (c) $x=0.2$, (d) $x=0.3$.

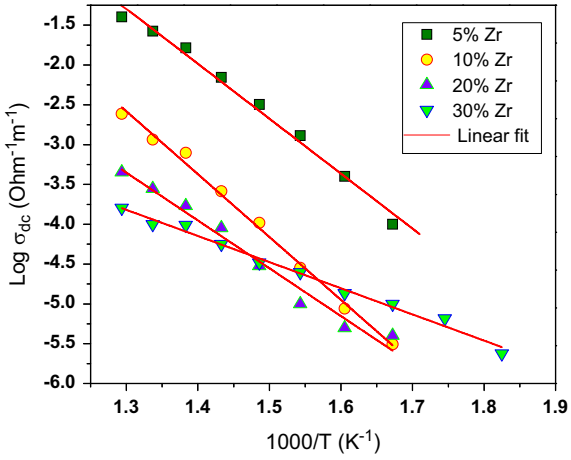


Fig. 6. Variation of dc conductivity with inverse of temperature of $(Na_{0.5}Bi_{0.5})Ti_{(1-x)}Zr_xO_3$, $x=0.0$, 0.05, 0.1, 0.2, 0.3.

$E_a$=activation energy and $k$=Boltzmann constant). The value of $E_a$ calculated from the slope of $\sigma_{dc}$ versus $10^3/T$ ($K^{-1}$) plot is given in Table 2. The value of activation energy indicates that the conduction in the materials may be due to the oxygen vacancies. This type of conduction by oxygen vacancy has been observed in many ferroelectric pervoskite oxides, and has been reported by various researchers [28–31]. The conduction due to oxygen vacancies in ferroelectrics is a collective phenomena rather than individual behavior. The oxygen vacancy concentration increases with increase in Zr concentration in NBT. The oxygen vacancies in ferroelectrics form "clusters" by the strong correlation among them [32]. These clusters of oxygen vacancy are distributed throughout ceramic samples. The energy required for the movement of such cluster is much lower than the energy required for the movement of individual oxygen vacancy. Thus the activation energy of the material may be due to the cluster formation of oxygen vacancies.

### 3.4. Impedance studies

The complex impedance spectroscopic (CIS) technique is used to analyze the electrical response of polycrystalline sample in a wide range of frequencies and temperature [33]. This technique is based on application of an alternating voltage signal to a sample and measurement of corresponding phase shifted current response. The complex impedance spectroscopy is a powerful tool to analyze the microstructure and properties relationship. The physical process occurring inside the sample can be modeled as an equivalent circuit using impedance spectra. The electrical ac response may be represented in any of the four basic formalisms via complex permittivity ($\varepsilon^*$), complex impedance ($Z^*$), complex admittance ($Y^*$) and complex electric modulus ($M^*$), which are interrelated to each other [34]. These relations offer a wide scope for a graphical

analysis of the various electrical parameters under different experimental conditions (temperature and frequency).

Fig. 7 shows the complex impedance graphs (Nyquist plot) of NBT and 5%, 10%, 20%, 30% Zr modified NBT ceramics at 400 °C. The linear relationship (straight line) is observed between real and imaginary part of impedance from room temperature to 275 °C suggesting the insulating property of the material. On and above 300 °C, a trend of formation of circular arc is started due to the increase in the grain and grain boundary microscopic conduction. This circular arc corresponds to the bulk property of the material. At higher temperatures, Nyquist plots seem to be overlapping of two semicircles. Each semicircle of the Nyquist plot corresponds to the different contributors of the samples to the electrical response. The semicircular arc of high frequency region can be attributed to the bulk (grain) property of the material arising due to a parallel combination of bulk resistance ($R_b$) and bulk capacitance ($C_b$) of the material. The semicircle arc at low frequency of the impedance spectrum (at elevated temperatures) is attributed to the presence of grain boundary arising due to a parallel combination of grain boundary resistance ($R_{gb}$)and capacitance ($C_{gb}$). The depressed nature of semicircular arc with the center lies below real impedance ($Z'$) axis suggests the relaxation process is non-ideal or non-Debye in nature [33]. This non-ideal behavior may be originated from several factors such as the grain orientation, grain size distribution, grain boundaries, atomic defect distribution, and stress–strain phenomena etc. [35]. The departure from ideal Debye behavior justifies the presence of a constant phase element (CPE) [36] in the equivalent circuit model for representing the materials electrical response. The CPE admittance is generally represented by $Y(\mathrm{CPE}) = A_0(j\omega)^n = A\omega^n + jB\omega^n$ [30] where $A = A_0\mathrm{Cos}(n\pi/2)$ and $B = A_0\mathrm{Sin}(n\pi/2)$. $A_0$ and $n$ are frequency independent but temperature dependent parameters, $A_0$ determines the magnitude of the dispersion and $n$ varies between zero and one ($0 \le n \le 1$). The CPE describes an ideal capacitor for $n=1$ and an ideal resistor for $n=0$. The equivalent circuit of two overlapping semicircular arcs of the impedance spectrum can be modeled by a series array of parallel combination of (i) a resistance (bulk resistance), capacitance (bulk capacitance) and a CPE, with another parallel combination of (ii) a resistance (grain boundary resistance), capacitance (grain boundary capacitance) as shown in Fig. 7 (below). Similar report is available in literature [7]. The impedance data (symbols) have been fitted (solid line) with the model (as described above) by commercially available software ZSIMP WIN Version 2 as shown in Fig. 7. It has been found that there is a close agreement between the observed and fitted values. The calculated $R_g$ and $R_{gb}$ values are given in Table 3. It can be seen from Table 3 that the value of grain resistance decreases with rise in temperature but it increases with increase of Zr content in NBT. As the grain resistance is large in comparison to the grain boundary, the impedance response is dominated by grain $RC$ element results in overlapped semicircular arc as shown in Fig. 7 [36]. The resistivity of grain boundaries are small in

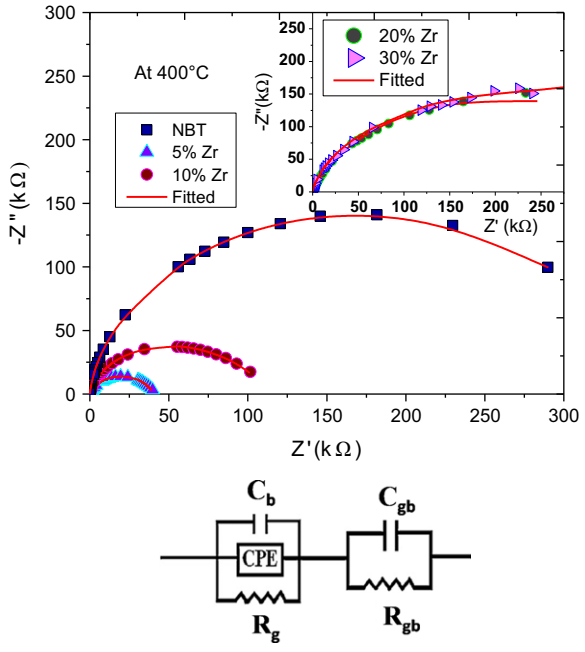


Fig. 7. Nyquist plots of $(Na_{0.5}Bi_{0.5})Ti_{(1-x)}Zr_xO_3$, $x=0.0$, 0.05, 0.1, 0.2, 0.3 at 400 °C. Equivalent circuit is shown below the figure.

Table 3
Model equivalent circuit fitted parameters $R_g$ (Ohm) and $R_{gb}$ (Ohm) of Zr modified NBT.

| Temperature (°C) | 5% Zr | | 10% Zr | | 20% Zr | | 30% Zr | |
|---|---|---|---|---|---|---|---|---|
| | $R_g$ | $R_{gb}$ | $R_g$ | $R_{gb}$ | $R_g$ | $R_{gb}$ | $R_g$ | $R_{gb}$ |
| **325** | 1,262,000 | – | 4,547,000 | – | 8,247,000 | – | 1,401,000 | – |
| **350** | 232,900 | 101,000 | 1,664,000 | – | 3,590,000 | – | 1,255,000 | – |
| **375** | 80,820 | 42,520 | 413,800 | 42,730 | 1,200,000 | – | 516,900 | 653,500 |
| **400** | 31,600 | – | 102,000 | 9298 | 430,600 | 528.1 | 356,900 | 246,100 |
| **425** | 20,630 | – | 44,550 | 3000 | 162,300 | 318.5 | 201,900 | 16,980 |
| **450** | 11,810 | 1289 | 14,330 | 1183 | 76,910 | 187.9 | 137,200 | 10,790 |
| **475** | 8289 | 470 | 9997 | 649 | 48,870 | 134.5 | 105,700 | 51.01 |
| **500** | 6270 | 207 | 4732 | 113.9 | 30,070 | 87.66 | 76,550 | 44.17 |

compared to grains, may be due to presence of vacancy and space-charge at the grain boundaries [37].

Fig. 8 shows the variation of imaginary part of impedance ($Z''$) as a function of frequency of NBT and Zr modified NBT at 400 °C. The values of $Z''$ monotonically decrease on increasing frequency (without getting any peak at low temperature). At higher temperatures, $Z''$–frequency plot shows peak at a certain frequency ($f_{max}$) due to the relaxation process in the material. The magnitude of $Z''$at the peak ($Z''_{max}$) decreases with increase in temperature and the corresponding $f_{max}$ shifts towards higher frequency with broadening of the peak. It may be due to the hopping of small polaron with reduction of electron–lattice coupling with rise in temperature [36]. The relaxation time ($\tau$) corresponding to the $f_{max}(2\pi f_{max}\tau = 1)$ decreases with increase in temperature. Hence the relaxation process is temperature dependant. The asymmetric broadening of the peak of $Z''$ with frequency plot suggests the presence of distributed relaxation process. The existence of distributed relaxations may be due to the fluctuation in the structure by the substitution of Bi, and Na in A-site and Zr, Ti in B-site of NBT. The observed relaxation peak position shift towards lower frequency indicating the increase of relaxation time and the value of ($Z''_{max}$) decreased with increase in Zr content in NBT at a constant temperature. All the curves for different compositions merge at high frequency region due to the release of space charges in the samples [38].

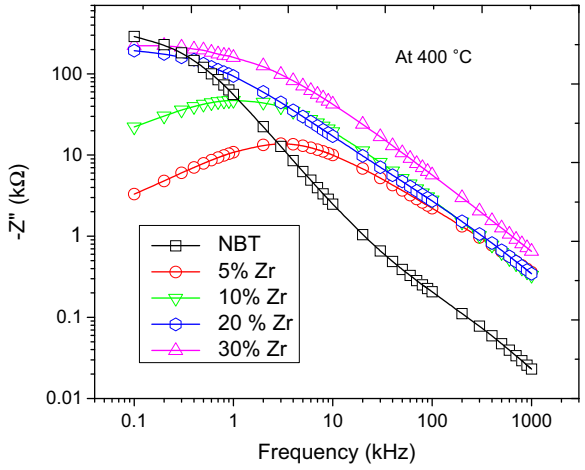


Fig. 8. Variation of $Z''$ with frequency of $(Na_{0.5}Bi_{0.5})Ti_{(1-x)}Zr_xO_3$, $x$=0.0, 0.05, 0.1, 0.2, 0.3 at 400 °C.

In the complex impedance plot, an overlapped semicircle is observed as the larger resistance of grain impedance response (parallel $RC$ element) is dominated over grain boundary. However, in the modulus formalism has advantage as it gives more emphasis on the capacitance.

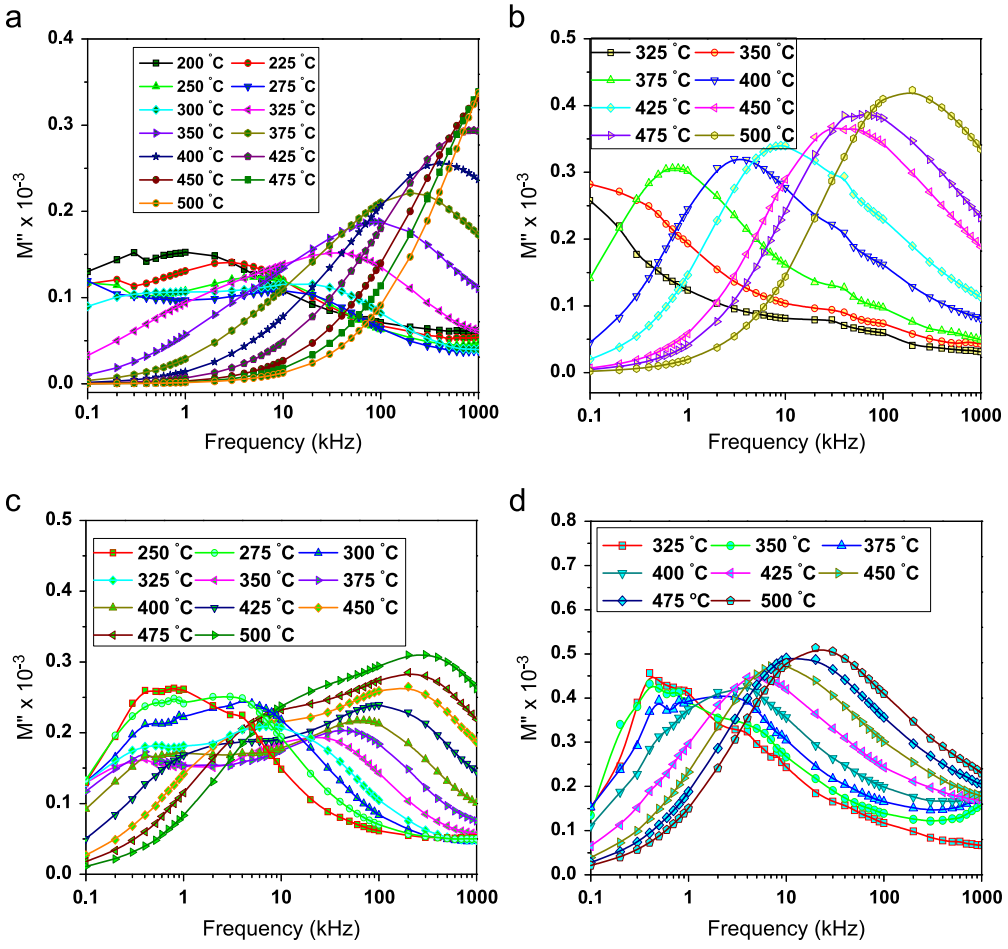


Fig. 9. Variation of $M''$ with frequency at various temperatures of $(Na_{0.5}Bi_{0.5})Ti_{(1-x)}Zr_xO_3$, (a) $x$=0.05, (b) $x$=0.1, (c) $x$=0.2, (d) $x$=0.3.

Fig. 9(a–d) shows the variation of imaginary electric modulus ($M''$) with frequency of 5%, 10%, 20% and 30% Zr modified NBT. The magnitude of $M''$ decreases with increase in frequency but at high temperatures a prominent peak appeared. This peak indicates the transition of long range to short-range mobility with increase in frequency. On low frequency side of the peak, ions are capable of moving long distances (i.e., successful hopping from one site to the neighboring sites). However, the ions are spatially confined to the potential wells that only execute localized motion within the well on high frequency side of the peak. The peak position shifts toward higher frequency side with increase in temperature. The relaxation time (corresponding to the frequency at $M''_{max}$) decreases with increase in temperature. Thus, the relaxation in non-localized process is temperature dependent. The magnitude of peak ($M''_{max}$) also varies with increase in temperature. Two well resolved relaxation phenomena are observed in all case except 10% Zr modified NBT. It confirms the presence of both grain (low frequency) and grain boundary (high frequency) phenomena in the material. The separation of two contributors in modulus spectrum may be due to the comparable capacitances of grain and grain boundary even though a large difference between their resistance contributions. The FWHM of the peak is observed to be more than that of Debye peak (1.14 decades). It also suggests that the relaxation process is non-Debye type. The peak shape of the M″ versus frequency plot is of asymmetric nature. This is due to the spread of relaxation time. Such behavior may be due to the non-exponential process, such as diffusive motion of the ions or non-uniform microstructure of the materials [39]. In the high frequency region, all the curves merge apparently into a single line. This is because of the long-range conductivity process in materials [40].

## 4. Conclusion

The Zr modified NBT polycrystalline powders were prepared by a high-temperature solid-state reaction technique. The formation of the materials was confirmed by preliminary X-ray diffraction analysis. The Zr modified NBT samples have rhombohedral crystal system with hexagonal axis. The grain size of the samples was found to be increased on Zr substitution in NBT. The phase transition has been clearly observed at high frequency whereas at low frequency it is masked by the space charge polarization of the materials. The maximum dielectric constant decreases and $T_{max}$ increases on incorporation of Zr at the Ti site of NBT. The diffusivity of the phase transition increases due to disordering created by Zr substitutions. The variation of ac conductivity with frequency obeys Jonscher power law. The material shows conductivity due to translational and localized hopping motion of charge carriers. Complex impedance spectroscopy confirmed the existence of non-Debye type of relaxation process in the materials which is contributed due to the grain and grain boundary effects. An equivalent circuit model has been proposed based on brick layer model for the observed electrical response of the sample. The grain and grain boundary resistance decrease with rise in temperature for all the samples

## Acknowledgments

Authors express sincere gratitude to the members of Ferroelectric Laboratory of the Department of Physics and Meteorology, Indian Institute of Technology Kharagpur 721302, India for help in some experimental work.

## References

[1] K. Uchino, Ferroelectric Devices, Marcel Dekker, Inc., New York, USA, 2000.
[2] J. Kulawik, D. Szwagierczak, B. Groger, Investigations of properties of ceramic materials with perovskite structure in chosen electronic applications, Bulletin of the Polish Academy of Sciences: Technical Sciences 55 (2007) 293–297.
[3] M.D. Maeder, D. Damjanovic, N. Setter, Lead free piezoelectric materials, Journal of Electroceramics 13 (2004) 385–392.
[4] C.F. Buhrer, Some properties of bismuth perovskites, Journal of Chemical Physics 36 (1962) 798–803.
[5] Chenggang Xu, Dunmin Lin, K.W. Kwok, Structure, electrical properties and depolarization temperature of $(Bi_{0.5}Na_{0.5})TiO_3$–$BaTiO_3$ lead-free piezoelectric ceramics, Solid State Sciences 10 (2008) 934–940.
[6] H. Zhang, S.J. Fu, W.J. Long, D.J. Guo, Temperature-dependent electrical properties of B-site zinc substituted bismuth sodium titanate piezoceramics, Ceramics International 38 (2012) 3237–3242.
[7] B.K. Barick, R.N.P. Choudhary, D.K. Pradhan, Phase transition and electrical properties of lanthanum-modified sodium bismuth titanate, Materials Chemistry and Physics 132 (2012) 1007–1014.
[8] A. Watcharapasorn, S. Jiansirisomboon, Dielectric and piezoelectric properties of zirconium-doped bismuth sodium titanate ceramics, Advanced Materials Research 55–57 (2008) 133–136.
[9] Y. Yuan, E.Z. Li, B. Li, B. Tang, X.H. Zhou, Effects of Ca and Mn additions on the microstructure and dielectric properties of $Na_{0.5}Bi_{0.5}TiO_3$ ceramics, Journal of Electronic Materials 40 (2011) 2234–2239.
[10] Y. Yamada, T. Akutsu, H. Asada, K. Nozawa, S. Hachiga, T. Kurosaki, O. Ikagawa, H. Fujiki, K. Hozumi, T. Kawamura, T. Amakawa, K. Hirota, T. Ikeda, Effect of B-Ions Substitution in $[(K_{1/2}Bi_{1/2})$–$(Na_{1/2}Bi_{1/2})](Ti$–$B)O_3$ system with B=Zr, $Fe_{1/2}Nb_{1/2}$, $Zn_{1/3}Nb_{2/3}$ or $Mg_{1/3}Nb_{2/3}$, Japanese Journal of Applied Physics 34 (1995) 5462–5466.
[11] Lily, K. Kumari, K. Prasad, R.N.P. Choudhary, Impedance analysis of $(Na_{0.5}Bi_{0.5})(Zr_{0.25}Ti_{0.75})O_3$ ceramic, Indian Journal of Engineering and Materials Sciences 15 (2008) 147–151.
[12] Lily, K. Kumari, K Prasad, K.L. Yadav, Dielectric and impedance study of lead-free ceramic: $(Na_{0.5}Bi_{0.5})ZrO_3$, Journal of Materials Science 42 (2007) 6252–6259.
[13] K. Kumari, K. Prasad, K.L. Yadav, S. Sen, Structural and dielectric properties of $ZrO_2$ added $(Na_{1/2}Bi_{1/2})TiO_3$ ceramic, Brazilian Journal of Physics 39 (2009) 297–300.
[14] S.A. Sheets, A.N. Soukhojak, N. Ohashi, Y.M. Chiang, Relaxor single crystals in the $(Bi_{1/2}Na_{1/2})_{1-x}Ba_xZr_yTi_{1-y}O_3$ system exhibiting high electrostrictive strain, Journal of Applied Physics 90 (2001) 5287–5289.
[15] A. Rachakom, P. Jaiban, S. Jiansirisomboon, A. Watcharapasorn, Crystal structure and electrical properties of bismuth sodium titanate zirconate ceramics, Nanoscale Research Letters 7 (2012) 57-1-5.

[16] E. Aksel, J.S. Forrester, B. Kowalski, M. Deluca, D. Damjanovic, J.L. Jones, Structure and properties of Fe-modified $Na_{0.5}Bi_{0.5}TiO_3$ at ambient and elevated temperature, Physical Review B 85 (2012) 024121–11.
[17] E. Aksel, H. Foronda, K.A. Calhoun, J.L. Jones, S. Schaab, T. Granzow, Processing and properties of $Na_{0.5}Bi_{0.5}TiO_3$ piezoelectric ceramics modified with La, Mn and Fe, Functional Materials Letters 3 (2010) 45–48.
[18] H. Yu, Z.G. Ye, Dielectric, ferroelectric, and piezoelectric properties of the lead-free $(1-x)(Na_{0.5}Bi_{0.5})TiO_{3-x}BiAlO_3$ solid solution, Applied Physics Letters 93 (2008) 112902–112903.
[19] G.H. Haertling, Ferroelectric ceramics: history and technology, Journal of the American Ceramic Society 82 (1999) 797–818.
[20] F. Moura, A.Z. Simoes, B.D. Stojanovic, M.A. Zaghete, E. Longo, J.A. Varela, Dielectric and ferroelectric characteristics of barium zirconate titanate ceramics prepared from mixed oxide method, Journal of Alloys and Compounds 462 (2008) 129–134.
[21] POWD—an Interactive Powder Diffraction Data Interpretation and indexing Program Version 2.2 by E. Wu, School of Physical sciences, Flinder University of South Australia Bedford Park, S.A. 5042, Australia.
[22] R. Selvamani, G. Singh, V. Sathe, V.S. Tiwari, P.K. Gupta, Dielectric, structural and Raman studies on $(Na_{0.5}Bi_{0.5}TiO_3)_{(1-x)}(BiCrO_3)_x$ ceramic, Journal of Physics: Condensed Matter 23 (2011) 055901–055908.
[23] G.K. Williumson, W.H. Hall, X-ray line broadening from filed aluminium and wolfram, Acta Metallurtica 1 (1953) 22–31.
[24] J.K. Lee, K.S. Hong, C.K. Kim, S.E. Park, Phase transitions and dielectric properties in A-site ion substituted $(Na_{1/2}Bi_{1/2})TiO_3$ ceramics (A=Pb and Sr), Journal of Applied Physics 91 (2002) 4538–4542.
[25] M.D. Glinchuk, I.P. Bykov, S.M. Kornienko, V.V. Laguta, A.M. Slipenyuk, A.G. Bilous, O.I. V'yunov, O.Z. Yanchevskii, Infuence of impurities on the properties of rare-earth-doped barium titanate ceramics, Journal of Materials Chemistry 10 (2000) 941–947.
[26] A.K. Jonscher, Dielectric relaxation in solids, Journal of Physics D: Applied Physics 32 (1999) R57.
[27] N. Ortega, A. Kumar, P. Bhattacharya, S.B. Majumder, R.S. Katiyar, Impedance spectroscopy of multiferroic $PbZr_xTi_{1-x}O_3/CoFe_2O_4$ layered thin films, Physical Review B: Condensed Matter 77 (014111) (2008) 1–10.
[28] B. Jiménez, J.M. Vicente, Oxygen defects and low-frequency mechanical relaxation in Pb–Ca and Pb–Sm titanates, Journal of Physics D: Applied Physics 31 (1998) 446–452.
[29] Z. Chen, L.E. Yu, Cross, Oxygen-vacancy-related low-frequency dielectric relaxation and electrical conduction in Bi:$SrTiO_3$, Physical Review B: Condensed Matter 62 (2000) 228–236.
[30] S.S.N. Bharadwaja, S.B. Krupanidhi, Growth and study of antiferroelectric lead zirconate thin films by pulsed laser ablation, Journal of Applied Physics 86 (1999) 5862–5869.
[31] A.P. Barranco, J.D.S. Guerra, R.L. Noda, E.B. Araújo, Ionized oxygen vacancy-related electrical conductivity in $(Pb_{1-x}La_x)(Zr_{0.90}Ti_{0.10})_{1-x/4}O_3$ ceramics, Journal of Physics D: Applied Physics 41 (2008) 215503.
[32] W. Li, A. Chen, X. Lu, J. Zhu, Collective domain-wall pinning of oxygen vacancies in bismuth titanate ceramics, Journal of Applied Physics 98 (2005) 024109-1-5.
[33] B.K. Barick, K.K. Mishra, A.K. Arora, R.N.P. Choudhary, D.K. Pradhan, Impedance and Raman spectroscopic studies of $(Na_{0.5}Bi_{0.5})TiO_3$, Journal of Physics D: Applied Physics 44 (2011) 355402–355410.
[34] I.M. Hodge, M.D. Ingram, A.R. West, Impedance and modulus spectroscopy of polycrystalline solid electrolytes, Journal of Electroanalytical Chemistry 74 (1976) 125–143.
[35] S. Sen, R.N.P. Choudhary, A. Tarafdar, P. Pramanik, Impedance spectroscopy study of strontium modified lead zirconate titanate ceramics, Journal of Applied Physics 99 (2006) 124114–124118.
[36] D.K. Pradhan, R.N.P. Choudhary, C. Rinaldi, R.S. Katiyar, Effect of Mn substitution on electrical and magnetic properties of $Bi_{0.9}La_{0.1}FeO_3$, Journal of Applied Physics 106 (2009) 024102–024110.
[37] C. Tian, S.W. Chan, Electrical conductivities of $(CeO_2)_{1-x}(Y_2O_3)_x$ thin films, Journal of the American Ceramic Society 85 (2002) 2222–2229.
[38] R.N.P. Choudhary, D.K. Pradhan, C.M. Tirado, G.E. Bonilla, R.S. Katiyar, Structural, dielectric and impedance properties of $Ca(Fe_{2/3}W_{1/3})O_3$ nanoceramics, Physica B 393 (2007) 24–31.
[39] J. Liu, C.G. Duan, W.G. Yin, W.N. Mei, R.W. Smith, J.R. Hardy, Large dielectric constant and Maxwell–Wagner relaxation in $Bi_{2/3}Cu_3Ti_4O_{12}$, Physical Review B 70 (2004) 144106–144107.
[40] A.R. James, S. Priya, K. Uchino, K. Srinivas, Dielectric spectroscopy of $Pb(Mg_{1/3}Nb_{2/3})O_3$–$PbTiO_3$ single crystals, Journal of Applied Physics 90 (2001) 3504–3508.